ELSEVIER

Journal of Organometallic Chemistry 623 (2001) 65–73

Journal of Organometallic Chemistry

www.elsevier.nl/locate/jorganchem

Formation of rhodium carbonyl thiolate dimers via elimination of dihydrogen; crystal and molecular structure of $[Rh_2(CO)_4(\mu\text{-}SC_6H_4CH_3)_2]$

Nitsa K. Kiriakidou-Kazemifar [a], Matti Haukka [b], Tapani A. Pakkanen [b], Sergey P. Tunik* [c,1], Ebbe Nordlander* [a,2]

[a] *Inorganic Chemistry 1, Chemical Center, Lund University, Box 124, SE-221 00 Lund, Sweden*
[b] *Department of Chemistry, University of Joensuu, PO Box 111, FIN-80101 Joensuu, Finland*
[c] *Department of Chemistry, St. Petersburg University, Universitetskii pr., 2, St. Petersburg 198904, Russian Federation*

Received 7 June 2000; accepted 5 September 2000

Abstract

Reaction of $[Rh_6(CO)_{15}(NCMe)]$ with *p*-thiocresol [(4-Me)C_6H_4SH] leads to the formation of $[Rh_2(CO)_4(\mu\text{-}SC_6H_4CH_3)_2]$ as the main product along with a small amount of $[Rh_6(CO)_{16}]$. An approximately 30-fold excess of the thiol is required in order to obtain a good yield of the thiolate-bridged dimer while reaction of $[Rh_4(CO)_{12}]$ with an excess of *p*-thiocresol leads to an apparently clean conversion to the dimeric Rh(I) complex. Mass spectrometric measurements show that the latter reaction involves evolution of H_2, and CO evolution is indicated by the retardation of the reaction in CO saturated solution; these results suggest the following reaction stoichiometry: $[Rh_4(CO)_{12}] + 4RSH \rightarrow 2[Rh_2(CO)_4(\mu\text{-}SR)_2] + 2H_2 + 4CO$. Kinetic measurements show that the reaction proceeds in three stages which are proposed to involve two rapid pre-equilibria and a final irreversible and relatively slow conversion to the products. The crystal and molecular structure of $[Rh_2(CO)_4(\mu_2\text{-}SC_6H_4CH_3)_2]$ is reported.

Keywords: Rhodium; Thiol; Cluster; Hydrodesulfurization; Mechanism

1. Introduction

The commercial and environmental importance of hydrodesulfurization (HDS) catalysis serves as an impetus for research on the mechanism(s) of desulfurization of thiols, thioethers and thiophenes in heterogeneous and homogeneous systems in which transition metal sulfides or coordination complexes serve as catalysts or stoichiometric reagents [1–4]. Because of the experimental difficulties encountered during in situ studies of commercial catalysts (Mo–Co–S or Mo–Ni–S phases) [2], the use of metal complexes and metal clusters has become an important alternative means to study HDS mechanisms [3–5]. We are currently involved in a broad study of coordination modes of sulfur-containing ligands to transition metal carbonyl clusters and the reactivity of metal carbonyl clusters containing such ligands. Our aims are to relate observed coordination modes to possible intermediates in HDS catalysis and to investigate the viability of using clusters as stoichiometric reagents (or catalysts) in homogeneous desulfurization reactions. Our efforts have thus far been concentrated on ruthenium and osmium clusters [6–8] as it has been shown that the sulfides of these two metals exhibit high HDS activity [2]. The activities of rhodium and iridium sulfides are comparable to those of ruthenium and osmium, and we have therefore begun to investigate the reactivities of rhodium clusters towards sulfur-containing ligands. Here, we wish to report the redox reactions of two rhodium carbonyl clusters with *p*-thiocresol, which in both cases lead to the formation of $[Rh_2(CO)_4(\mu_2\text{-}SC_6H_4CH_3)_2]$. Reaction of the thiol with $[Rh_4(CO)_{12}]$ leads to the formation of the dimeric product in high

[1] *Corresponding author.
[2] *Corresponding author. Tel.: +46-46-108118; fax: +46-46-2224439; e-mail: ebbe.norlander@inorg.lu.se

0022-328X/01/$ - see front matter
PII: S0022-328X(00)00657-4

yield with concomitant evolution of dihydrogen. A preliminary investigation of the kinetics of the latter redox reaction and a proposal for its mechanism is also described.

2. Experimental

The clusters $[Rh_4(CO)_{12}]$ [9] and $[Rh_6(CO)_{15}(NCMe)]$ [10] were prepared by literature methods. *para*-Thiocresol (Lancaster Chemicals), tetrabutylammonium bromide (Acros) and carbon monoxide (AGA) were used as received. All reactions were carried out under an atmosphere of dry, oxygen free nitrogen (unless otherwise stated), using solvents which were freshly distilled from appropriate drying agents. Infrared spectra were recorded in n-hexane or dichloromethane solution in 0.5 mm NaCl cells, using a Nicolet Avatar FTIR spectrometer. ^{1}H-NMR spectra were recorded on a Varian Unity 300 MHz spectrometer using the solvent resonance as an internal standard. Thin layer chromatography was performed on commercial plates precoated with Merck Kieselgel 60–0.5 mm thickness. Products are given in order of decreasing R_f values. Fast atom bombardment (FAB^+) and electron impact (EI^+) ionization mass spectra were obtained on a JEOL SX-102 instrument. The matrix for the FAB^+ spectra consisted of 3-nitrobenzyl alcohol and CsI was used as calibrant. The EI^+ spectra were obtained using a PLOT 5 Å molecular sieve column (30 m × 0.32 mm × 30 mm) and CO as the carrying gas. All kinetic runs were monitored with an Applied Photophysics SX.18MV stopped flow spectrophotometer interfaced with a PC driven by PC Pro-K software. The temperature was maintained constant at 303 K with a Lauda RM6 thermostat bath.

2.1. Reaction of $[Rh_6(CO)_{15}(NCMe)]$ with p-thiocresol [(4-Me)C_6H_4SH]

A total of 170 mg of *p*-thiocresol (1.35 mM) were dissolved in 30 ml of dichloromethane and 35 mg of solid $[Rh_6(CO)_{15}(NCMe)]$ (0.032 mM) were added to the solution. The reaction mixture was left stirring for 4 h at room temperature (r.t.) after which the solution was concentrated to a minimal amount and separated by TLC using a hexane–dichloromethane mixture (5:1, *v*:*v*) as eluant. Two products were detected and isolated: dark reddish-brown $[Rh_2(CO)_4(\mu\text{-}SC_6H_4CH_3)_2]$ (**1**) (32 mg, 0.057 mmol) and $[Rh_6(CO)_{16}]$ (8 mg, 7.5 μmol). $Rh_2(CO)_4(\mu\text{-}SC_6H_4CH_3)_2$ (**1**) IR [ν_{CO} (cm^{-1}), CH_2Cl_2]: 2081w, 2063s, 2015s, 1963sh; ^{1}H-NMR [δ (ppm), $CDCl_3$]: 7.62 [d, ($SC_6H_4CH_3$), 2H], 7.07 [d, ($SC_6H_4CH_3$), 2H], 2.33 [s, ($SC_6H_4CH_3$), 3H], MS [FAB^+, m/z, amu] 565 (M^+), loss of 4 CO observed.

2.2. Reaction of $[Rh_4(CO)_{12}]$ with p-thiocresol

$[Rh_4(CO)_{12}]$ (40 mg, 0.05 mmol) was dissolved in hexane (20 ml) and solid *p*-thiocresol (53 mg, 0.43 mmol) was added to the solution. The mixture was stirred under nitrogen until no ν_{C-O} resonances of the starting material could be detected by IR spectroscopy. The solution was concentrated under reduced pressure and subjected to preparative TLC (dichloromethane–hexane, 2:3, *v*:*v*) to give $[Rh_2(CO)_4(\mu\text{-}SC_6H_4CH_3)_2]$ (**1**) (56 mg, 93%) as the main product. Trace amounts of two other yellow compounds with lower R_f than **1** were detected but were not characterized.

2.3. Detection of evolution of dihydrogen during the reaction of $[Rh_4(CO)_{12}]$ with p-thiocresol

Solid $[Rh_4(CO)_{12}]$ (50 mg, 0.07 mmol) and [(4-M_e) C_6H_4SH] (66 mg, 0.54 mmol) was put into one compartment of a 'double-horn' Schlenk vessel, and 20 ml of hexane into the other one. The hexane was degassed using freeze–pump–thaw techniques and the vessel was filled with CO (the use of argon or nitrogen as an inert component of the system would make it impossible to carry out the chromatography of the gas phase as described below). The reaction was started by transferring hexane into the compartment of the Schlenk vessel which contained the solid reagents. The mixture was stirred for 1 h, and heated to + 50°C to transfer gaseous products from solution into gas phase. A sample of the gas-phase was removed with a syringe and injected into a mass spectrometer at 50°C (EI^+). The composition of the gas-phase was analyzed by GC–MS which unambiguously displayed the peak of H_2. A control experiment was performed under exactly the same conditions, but in the absence of $[Rh_4(CO)_{12}]$ — no peak due to H_2 could be detected in this case.

2.4. Monitoring of the reaction of $[Rh_4(CO)_{12}]$ with p-thiocresol

2.4.1. IR

A 20-fold excess of *p*-thiocresol was added to a 0.13 mM solution of $[Rh_4(CO)_{12}]$ in hexane which was prethermostated to 30°C. The resultant solution was put into an IR cell and the reaction course was monitored by IR in the 2200–1500 cm^{-1} range. A clean conversion of $[Rh_4(CO)_{12}]$ into $[Rh_2(CO)_4(\mu\text{-}SC_6H_4CH_3)_2]$ (**1**) was observed.

2.4.2. Stopped-flow spectrometry

Kinetic runs were carried out in hexane under pseudo-first-order conditions using at least 20-fold excess of the thiol. The $[Rh_4(CO)_{12}]$ concentration used in all experiments was 1.2×10^{-4} M. The reaction course

Table 1
Crystal data and structure refinement for $[Rh_2(CO)_4(\mu\text{-}SC_6H_4CH_3)_2]$ (**1**)

Chemical formula	$C_{18}H_{14}O_4Rh_2S_2$
Molecular weight (g mol^{-1})	564.23
Crystal size (mm)	$0.3\times0.2\times0.05$
Color	Orange–red
Crystal system	Triclinic
Space group	$P\bar{1}$
Unit cell dimensions	
a (Å)	8.912(18)
b (Å)	9.975(2)
c (Å)	12.623(3)
α (°)	68.37(3)
β (°)	78.62(3)
γ (°)	71.25(3)
V (Å^3)	983.8(3)
Z	2
D_{calc} (Mg m^{-3})	1.905
Absorption coefficient μ (mm^{-1})	1.909
$F(000)$	552
θ range (°)	3.91–27.46
h range	−11–11
k range	−12–12
l range	−16–16
No. of collected reflections	8057
No. of unique reflections	4090
No. of observed reflections [a]	3678
No. of parameters	291
Final R indices [a]	0.0238
wR_2 [a]	0.0593
Goodness-of-fit	1.080
T (K)	120(2)

[a] $I>2\sigma(I)$, $w=1/[\sigma^2(F_o^2)+(xP)^2+yP]$, $P=(F_o^2+2F_c^2)/3$.

was followed by monitoring absorbance changes at 400 nm by stopped flow spectrometry. The reaction kinetics were studied in two time intervals, 0–20 and 0–500 s, for each concentration of the thiol ligand. The frequency of the data acquisition was varied in the ranges 0–2, 2–20 s, and 0–20, 20–500 s, respectively, in order to acquire maximum amount of points for each reaction stage. The first two stages, which were complete in 2 and 60 s, respectively, were accompanied by relatively small changes in the absorbance at 400 nm, while the final stage was accompanied by substantial UV absorbance changes and was assigned to final product accumulation. The observed rate constants for the three reaction steps were obtained by treatment of the data from the time intervals 0–2, 0–20 and 0–500 s using double exponential analysis to take into account overlapping successive kinetics. In order to investigate the effect of carbon monoxide on the rate of the reaction, one kinetic run was carried out in a CO saturated solution; CO was bubbled through solutions of both reagents for 15 min prior to the start of the reaction.

2.5. X-ray data collection and structure solution for $[Rh_2(CO)_4(\mu\text{-}SC_6H_4CH_3)_2]$ (1)

Single crystals of **1** suitable for X-ray analysis were obtained by slow evaporation of a pentane solution of the complex at r.t. The X-ray data was collected at 120 K on a Nonius Kappa CCD diffractometer using ϕ-scans [11] and Mo K_α radiation ($\lambda=0.71073$ Å). The cell refinement and data reduction were carried out using the Denzo and Scalepack programs [12]. The structure was solved by direct methods using SHELXS97 [13] and structure refinement was carried out with the SHELXL97 program [14]. All non-hydrogen atoms were refined anisotropically. Hydrogens were located from the difference Fourier map and refined isotropically.

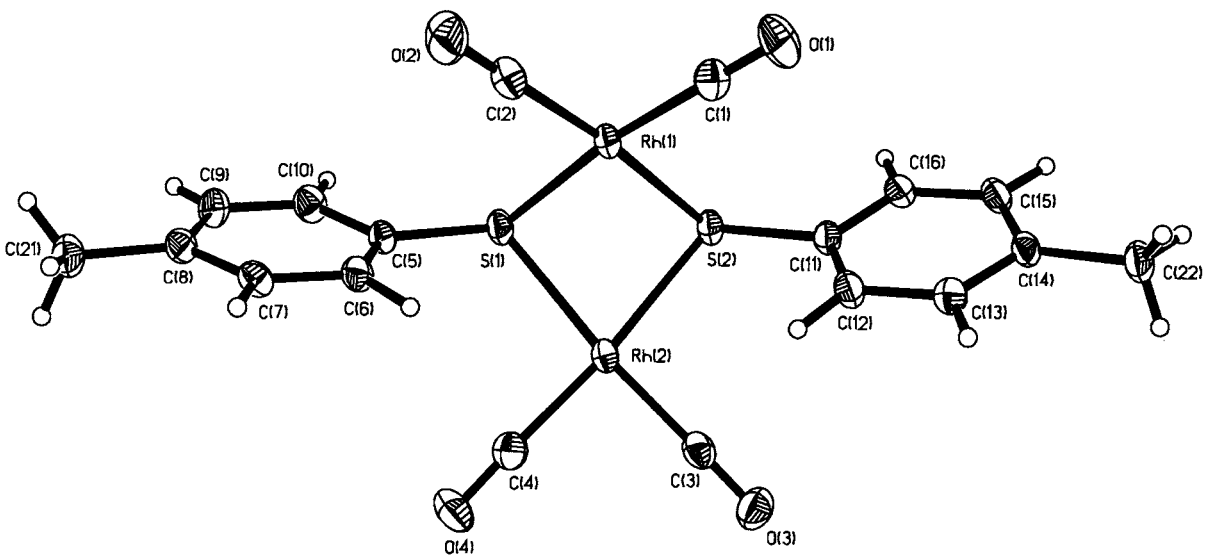

Fig. 1. An ORTEP plot of the molecular structure of $[Rh_2(CO)_4(\mu\text{-}SC_6H_4CH_3)_2]$ (**1**) showing the atom labeling scheme. Thermal ellipsoids are drawn at the 50% probability level.

Table 2
Selected bond lengths (Å) and angles (°) for $[Rh_2(CO)_4(\mu\text{-}SC_6H_4CH_3)_2]$ (**1**)

Bond lengths	
Rh(1)–C(1)	1.880(3)
Rh(1)–S(1)	2.3504(8)
Rh(1)–S(2)	2.3571(11)
Rh(1)–Rh(2)	3.1041(7)
Rh(2)–C(3)	1.869(3)
Rh(2)–C(4)	1.880(3)
Rh(2)–S(1)	2.3662(12)
Rh(2)–S(2)	2.3701(10)
C(1)–O(1)	1.132(3)
C(2)–O(2)	1.133(4)
C(3)–O(3)	1.131(3)
C(4)–O(4)	1.134(3)
Bond angles	
C(2)–Rh(1)–C(1)	91.38(12)
C(2)–Rh(1)–S(1)	95.68(8)
C(1)–Rh(1)–S(1)	172.39(9)
C(2)–Rh(1)–S(2)	173.92(8)
C(1)–Rh(1)–S(2)	93.93(9)
S(1)–Rh(1)–S(2)	78.87(3)
C(2)–Rh(1)–Rh(2)	125.05(8)
C(1)–Rh(1)–Rh(2)	123.98(9)
S(1)–Rh(1)–Rh(2)	49.06(3)
S(2)–Rh(1)–Rh(2)	49.14(3)
C(3)–Rh(2)–C(4)	90.75(12)
C(3)–Rh(2)–S(1)	170.62(9)
C(4)–Rh(2)–S(1)	96.37(9)
C(3)–Rh(2)–S(2)	94.84(8)
C(4)–Rh(2)–S(2)	174.04(9)
S(1)–Rh(2)–S(2)	78.30(3)
C(3)–Rh(2)–Rh(1)	130.37(8)
C(4)–Rh(2)–Rh(1)	125.51(9)
S(1)–Rh(2)–Rh(1)	48.62(2)
S(2)–Rh(2)–Rh(1)	48.77(3)
C(5)–S(1)–Rh(1)	111.56(9)
C(5)–S(1)–Rh(2)	116.13(9)
Rh(1)–S(1)–Rh(2)	82.31(3)
C(11)–S(2)–Rh(1)	109.15(9)
C(11)–S(2)–Rh(2)	114.53(9)
Rh(1)–S(2)–Rh(2)	82.09(3)

Relevant crystallographic data are summarized in Table 1.

3. Results and discussion

3.1. Reaction of $[Rh_6(CO)_{15}(NCMe)]$ with p-thiocresol

We have earlier reported on the reaction of the labilized cluster $[Os_3(CO)_{11}(NCMe)]$ with thiols to form products of the general formula $[(\mu\text{-}H)Os_3(CO)_{10}(\mu\text{-}SR)]$; this reaction proceeds via the formation of an intermediate which contains an agostic Os–H–SR interaction [7]. It is known that the reactivity of $[Rh_6(CO)_{15}(NCMe)]$ is similar to that of $[Os_3(CO)_{11}(NCMe)]$ in that substitution of the labile acetonitrile ligand proceeds via a dissociative pathway for both clusters, leaving a coordinatively unsaturated and two-electron deficient intermediate which readily reacts with nucleophiles [15,16]. In an attempt to detect a putative agostic intermediate of the form $[Rh_6(CO)_{15}(RSH)]$, $[Rh_6(CO)_{15}(NCMe)]$ was reacted with *p*-thiocresol in dichloromethane solution. In the presence of considerable excess of the thiol the main product of this reaction was identified as $[Rh_2(CO)_4(\mu_2\text{-}SC_6H_4CH_3)_2]$ (**1**) on the basis of its IR, NMR and mass spectra, which were similar to previously prepared $[Rh_2(CO)_4(\mu_2\text{-}SR)_2]$ compounds [17–23]. In addition, it was possible to grow crystals of **1** suitable for X-ray analysis and the solid state structure of **1** was determined by a single-crystal X-ray diffraction study (vide infra).

The outcome of the reaction of $[Rh_6(CO)_{15}(NCMe)]$ is dependent on the relative amount of thiol. The parent cluster, $[Rh_6(CO)_{16}]$ is always formed as a side product, even when a 30-fold excess of the thiol is used. The use of only a slight (1.5-fold) excess of the ligand results in a very low yield ($< 10\%$) of $[Rh_2(CO)_4(\mu_2\text{-}SC_6H_4CH_3)_2]$ while the main product is $[Rh_6(CO)_{16}]$. In the latter reaction, conversion of the starting material to $[Rh_6(CO)_{16}]$ occurs in 40 min at r.t. In the absence of thiol, the relatively labile $[Rh_6(CO)_{15}(NCMe)]$ is transformed into $[Rh_6(CO)_{16}]$ in an intermolecular CO 'redistribution' reaction which leads to approximately 50% conversion in approximately 24 h at r.t. [24]. It is plausible that the reaction of $[Rh_6(CO)_{15}(NCMe)]$ with thiol is of a bimolecular nature where an initial labile $[Rh_6(CO)_{15}(RSH)]$ species undergoes a redistribution/disproportionation reaction to form $[Rh_6(CO)_{16}]$ in the presence of relatively small concentrations of free thiol, while in the presence of a relatively large excess of the thiol, further reaction of $[Rh_6(CO)_{15}(RSH)]$ with thiol to form **1** occurs.

3.2. Crystal and molecular structure of $[Rh_2(CO)_4(\mu_2\text{-}SC_6H_4CH_3)_2]$ (1)

The molecular structure of $[Rh_2(CO)_4(\mu_2\text{-}SC_6H_4CH_3)_2]$ (**1**) is shown in Fig. 1; crystallographic data and selected bond lengths and angles are given in Table 2. The structure of **1** closely resembles those of $[Rh_2(CO)_4(\mu\text{-}SR)_2]$ (R = Ph, Et [22], SC_6H_4F [23]). Two thiolate bridges join the two rhodium atoms to form a central wingtip Rh_2S_2 fragment; the conformation of the molecule may be described as a bent *syn*, *endo* structure, the latter notation referring to the relative orientation of the thiolate substituents with respect to each other and the metal ligands, respectively [25]. The sulfur atoms are coordinated to the Rh_2 center in a slightly asymmetric manner, the differences between the long and short metal–sulfur bonds for two sulfur atoms is 0.015 and 0.013 Å. The Rh_2S wings of the central core form a dihedral angle of 114.4°, which is very close

to the values found for the two crystallographically independent molecules in $[Rh_2(CO)_4(\mu\text{-}SC_6H_5)_2]$ (115.2 and 113.7°, respectively [22]). The Rh–Rh intramolecular distance, 3.104(1) Å, is slightly longer than those in $[Rh_2(CO)_4(\mu_2\text{-}SR)_2]$ (R = Ph: $Rh\text{–}Rh_{av} = 3.092$ Å; C_6H_4F: $Rh\text{–}Rh_{av} = 3.073$ Å). These distances are longer than usual Rh–Rh bonding contacts in cluster compounds, e.g. 2.73 Å in $[Rh_4(CO)_{12}]$ [26] and 2.78 Å in $[Rh_6(CO)_{16}]$ [27] and imply a very weak Rh–Rh interaction, if any. A recent calculational study indicates that the molecular energy is stabilized by a weak Rh–Rh interaction in the model $[Rh_2(CO)_4(\mu\text{-}SH)_2]$ [25]. On the other hand, it should be noted that the intermetal distance in $[Rh_2(CO)_4(\mu\text{-}SEt)_2]$ [22], 2.820(2) Å, is consistent with a metal–metal bond. The angular parameters of the ligand environment of each rhodium atom range from 90.8 to 96.4° for the C–Rh–C and C–Rh–S bond angles and are equal to 78.9 and 78.3° for the S–Rh–S angles. Deviations of the ligands from idealized planar arrangement are rather small and do not exceed 0.05 Å. Thus, the rhodium atoms are in slightly distorted square planar coordination geometries, in accordance with their formal oxidation states of +1 (d^8).

3.3. Reaction of $[Rh_4(CO)_{12}]$ with p-thiocresol

Previous syntheses of $[Rh_2(CO)_4(\mu_2\text{-}SR)]$ complexes [17–20] involve reaction of $[Rh_2(CO)_4Cl_2]$ with thiols

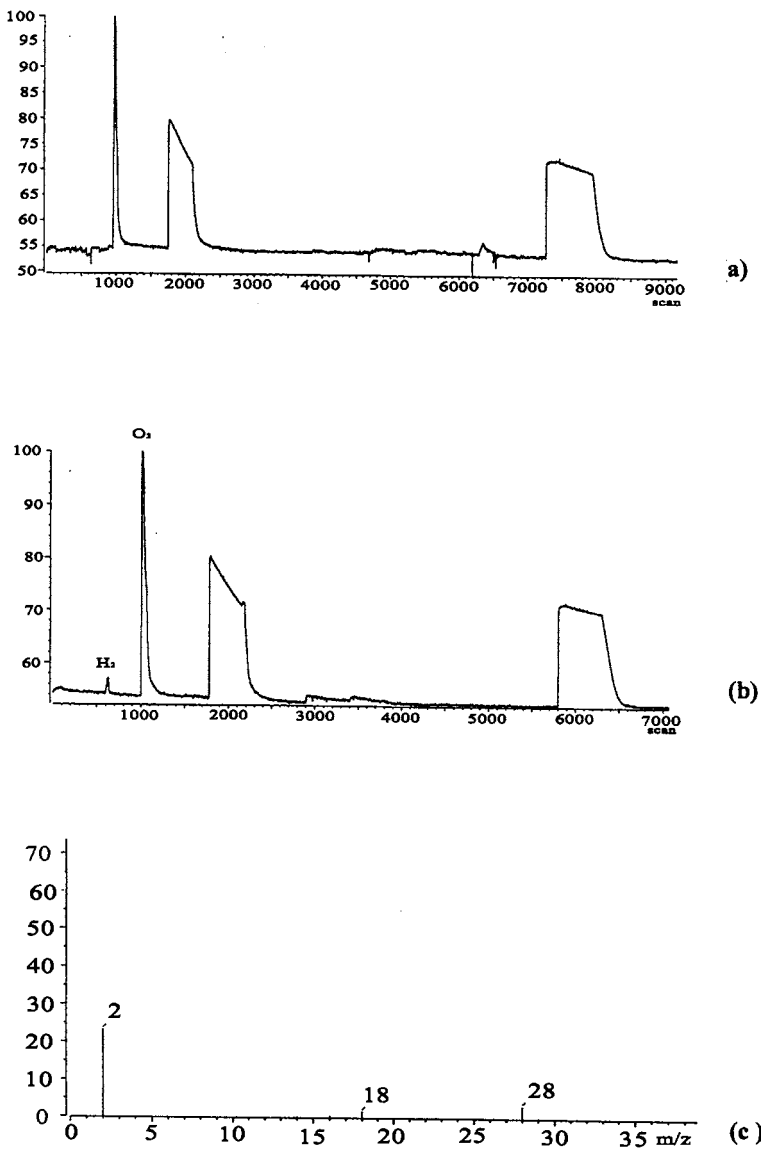

Fig. 2. (a) GC trace of blank experiment for detection of hydrogen gas (cf. Section 2.3). (b) GC trace of gaseous products from the reaction of $[Rh_4(CO)_{12}]$ with *p*-thiocresol. (c) Mass spectrum showing the presence of H_2 ($m/z = 2$ amu), H_2O (18 amu, artifact) and CO (28 amu, carrier gas) in the above-mentioned reaction.

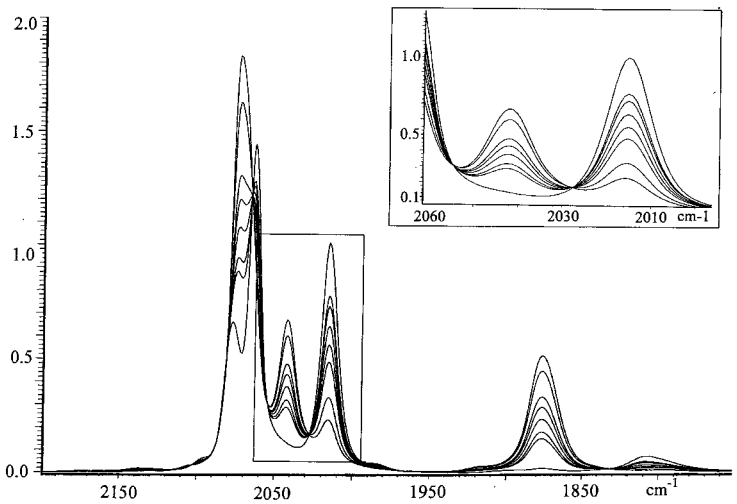

Fig. 3. Time-resolved IR spectra for the reaction of $[Rh_4(CO)_{12}]$ with *p*-thiocresol. An expansion of the 2060–2000 cm^{-1} region (inset) shows two of the isosbestic points at approximately 2055 and 2026 cm^{-1}. The spectra have been collected with a resolution of 2 cm^{-1} and smoothed using a Savitsky–Golay algorithm [34].

resulting in substitution of the bridging chlorides by thiolate moieties. The concomitant HCl evolution appears to be a thermodynamic driving force for this reaction; the thiolate complexes that are formed are relatively unstable in comparison with the parent chloride derivative [17,19]. Reaction of $[Rh_4(CO)_{12}]$ with *p*-thiocresol in hexane or dichloromethane at r.t. also leads to an apparently clean and quantitative conversion to $[Rh_2(CO)_4(\mu_2\text{-SR})]$ (**1**). The presence of atmospheric oxygen does not display any effect on the composition of the reaction products and the reaction rate (vide infra). It has been proposed that reactions of mono-, di- and trinuclear iron carbonyl compounds [28–30] and $[M_3(CO)_{12}]$ (M = Ru, Os) [31] to form metal carbonyl thiolate clusters proceeds via evolution of H_2; however, direct detection of dihydrogen has hitherto not been observed in such reactions. In order to confirm that H_2 is indeed formed in the reaction of $[Rh_4(CO)_{12}]$ with *p*-thiocresol, the reaction system was monitored by GC–MS (cf. Section 2.3). The results unambiguously show that H_2 is formed during the reaction while a blank experiment (cf. Section 2.3) did not display any detectable evolution of dihydrogen (Fig. 2). It thus appears that the reaction stoichiometry may be summarized by Eq. (1).

$$[Rh_4(CO)_{12}] + 4RSH \rightarrow 2[Rh_2(CO)_4(\mu\text{-SR})_2] + 2H_2 + 4CO \quad (1)$$

3.4. Kinetic/mechanistic studies

In order to gain insight into the mechanistic features of Reaction (1), a preliminary kinetic study has been undertaken. Monitoring of the reaction by IR spectroscopy indicates clean conversion of $[Rh_4(CO)_{12}]$ into $[Rh_2(CO)_4(\mu\text{-SR})_2]$ with isosbestic points at 2026, 2055 and 2078 cm^{-1} remaining throughout the reaction (Fig. 3). The reaction was monitored at 2069 and 2063 cm^{-1}, respectively ($[L] = 3.2 \times 10^{-3}$ M), and a kinetic curve was obtained. The observed rate constants were obtained using single exponential analysis and an average value was calculated ($k_{obs} = 0.004$ s^{-1}). No IR resonances other than those attributable to the starting material and the product could be detected. Thus, no appreciable amounts of any intermediate species could be detected by IR spectroscopy under the time scale applied (0–900 s). Neither could any hydride or other intermediate species be detected by ^{1}H-NMR spectroscopy.

However, kinetic results obtained using stopped flow techniques showed that Reaction (1) is a multistage process, which includes two sequential preequilibria and a final irreversible process to form the binuclear product. These three successive stages of the reaction have been detected in various time intervals; experimental kinetic curves along with the corresponding fits are shown in Fig. 4. At 303 K and $[Rh_4(CO)_{12}] = 1.2 \times 10^{-4}$ M, the first two stages are complete in 2 and 60 s, respectively, while the third, relatively slow stage occurs in the 60–900 s time interval, which is in agreement with the above-mentioned IR experiments. The kinetic parameters for these three stages were obtained using double exponential analysis to avoid 'mixing effects' of the sequential reaction kinetics; the rate constants obtained at various ligand concentrations are given in Table 3. The rate constants for the first two stages appear to be independent of ligand concentration while the rate constant for the third increases slightly with increasing ligand concentration. Further studies covering a wider thiol concentration range are currently

being undertaken; these studies confirm the dependence of the rate of the third stage on the thiol concentration [33]. The absence of a dependence of the first two observed rate constants on ligand concentration implies unimolecular rate determining steps for both reactions. It is likely that these reactions involve activation of the cluster by, for example, CO dissociation or metal–metal bond scission, to generate vacant coordination sites. The observed rate constant for the third stage, which is derived from stopped-flow measurements ($k_{obs} = 3.2 \times 10^{-3}$ s^{-1}, [L] $= 2.5 \times 10^{-3}$ M), is close to that obtained via IR spectroscopy (vide supra) within the limits of experimental uncertainty. The reaction scheme depicted in Scheme 1 may explain the experimental observations.

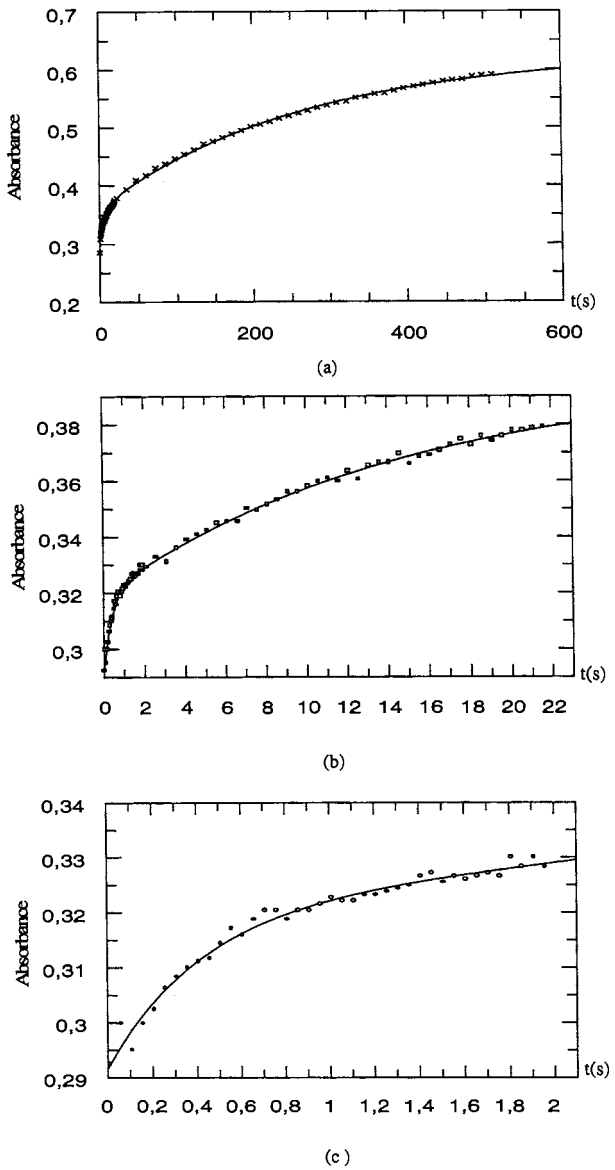

Fig. 4. Kinetic traces for the three stages detected in the reaction of $[Rh_4(CO)_{12}]$ with *p*-thiocresol at 303 K; $[Rh_4(CO)_{12}] = 1.2 \times 10^{-4}$ M, $[SC_6H_4CH_3] = 1 \times 10^{-2}$ M. Observed data (× , □, ○) and theoretical fits (solid lines) for (a) all three stages (0–600 s) (b) the first and second stage (0–24 s) (c) the first stage (0–2 s).

Table 3
Rate constants for the reaction of $[Rh_4(CO)_{12}]$ [a] and *p*-thiocresol in hexane [b]

$[HSC_6H_4CH_3]$ (mol dm^{-3})	k_{obs1} (s^{-1})	k_{obs2} (s^{-1})	k_{obs3} (s^{-1})
0.003 (IR monitoring) [c]			0.004 ± 0.001
0.0025	3.08 ± 0.17	0.056 ± 0.004	0.0032 ± 0.0001
0.005	2.44 ± 0.18	0.067 ± 0.005	0.0037 ± 0.0002
0.01	2.57 ± 0.12	0.065 ± 0.003	0.0037 ± 0.0001
0.01 (CO saturated solutions)			0.0023 ± 0.002
0.02	2.33 ± 0.24	0.051 ± 0.002	0.0050 ± 0.0002

[a] $[Rh_4(CO)_{12}] = 1.2 \times 10^{-4}$ M.
[b] Temperature = 303 K, $\lambda = 400$ nm.
[c] $[Rh_4(CO)_{12}] = 1.3 \times 10^{-4}$ M.

For the three detected reaction stages, each subsequent step is slower than the preceding one (cf. Table 3). This should normally result in accumulation of reaction products from each stage of the reaction and it should thus be possible to observe reaction intermediates but, as previously mentioned, no intermediates could be detected by IR spectroscopy. This fact along with the isosbesticity of the obtained spectra implies a very low concentration of the products formed in stages A and B of Scheme 1. The proposed mechanism can match the experimental data if both the A and B stages are completely reversible and the equilibria are shifted to the left, i.e. $k_1^{A,B}$, $k_{-2}^{A,B} \ll k_2^{A,B}$, $k_{-2}^{A,B}$; this also explains the low concentration of the intermediates formed in these stages. The shift of the equilibria is in agreement with the expected lability of the thiol ligand in the coordination sphere of the Rh_4 cluster. The reversibility of the A and B stages does not prevent single exponential treatment of the kinetics of each individual stage; however, the observed rate constants are in this case a combination of the constants for the forward and back reactions. The above-mentioned assumptions imply that the k_{obs} values for the A and B stages should be independent of ligand concentration, as is observed experimentally. It should be noted that the present data does not permit the distinction between intermediates of a dissociative nature, e.g. '$[Rh_4(CO)_{11}]$', '$[Rh_4(CO)_{10}(HSR)]$', and intermediates that are formed by opening of the cluster framework/metal–metal bond scission, e.g. '$[Rh_4(CO)_{12}]$*', '$[Rh_4(CO)_{11}(HSR)]$*' ('butterfly' clusters).

In order to probe whether carbon monoxide retards the reaction between $[Rh_4(CO)_{12}]$ and *p*-thiocresol, the kinetics of the reaction in CO saturated hexane solution were studied by stopped-flow spectrometry. Under

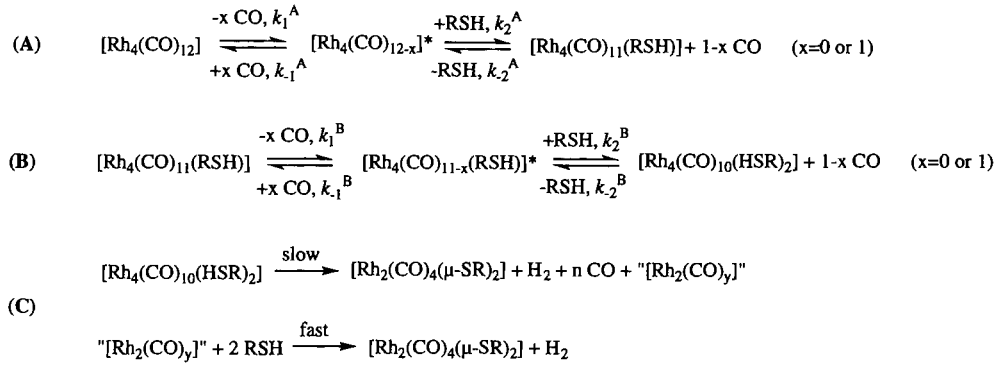

Scheme 1. Proposed mechanism for the reaction of $[Rh_4(CO)_{12}]$ with *p*-thiocresol.

these conditions, only a slow reaction that could be fitted to a single exponential function could be detected ($k_{obs} = 2.3 \times 10^{-3}$ s^{-1} for $[RSH] = 0.01$ M, $[Rh_4(CO)_{12}] = 1.2 \times 10^{-4}$ M); this observation is in agreement with Scheme 1. The presence of excess CO shifts the A and B equilibria further to the left, making the corresponding UV absorbances negligible and preventing detection of the two initial stages of the reaction. The observed rate constant, which thus corresponds to the third stage of the reaction, is considerably smaller than that measured in the absence of CO.

We propose that the intermediate that is formed as a product in equilibrium B is $[Rh_4(CO)_{10}(RSH)_2]$. A possible mechanism for subsequent formation of dihydrogen involves oxidative addition of an S–H bond at a Rh center or across a Rh–Rh bond to generate a thiolate ligand and a hydride. The very low affinity of $[Rh_4(CO)_{12}]$ and $[Rh_6(CO)_{16}]$ towards hydrides is well known and a hydride species is therefore expected to be labile [32]; the hydride may combine with the proton of the second (coordinated) thiol to form H_2. The dihydrogen evolution is accompanied by the formation of two thiolate bridges and cluster core cleavage to afford the binuclear Rh(I) product and a coordinatively unsaturated $[Rh_2(CO)_y]$ species. The latter species subsequently adds two further thiol ligands and undergoes a reaction sequence similar to that described to complete the reaction stoichiometry (cf. Scheme 1).

4. Summary and conclusions

Reaction of $[Rh_6(CO)_{15}(NCMe)]$ with a large excess of *p*-thiocresol leads to the formation of $[Rh_2(CO)_4(\mu\text{-}SC_6H_4\text{-}p\text{-}Me)]$. On the other hand, the presence of a relatively low concentration of thiol appears to catalyze the conversion of $[Rh_6(CO)_{15}(NCMe)]$ into $[Rh_6(CO)_{16}]$ in a CO redistribution reaction. Reaction of the thiol with $[Rh_4(CO)_{12}]$ leads to *quantitative* conversion to $[Rh_2(CO)_4(\mu\text{-}SC_6H_4\text{-}p\text{-}Me)]$ with concomitant H_2 evolution, and CO evolution is indicated by the retardation of the reaction rate(s) in CO-saturated solution. These observations are in accordance with the stoichiometry in Eq. (1) (vide supra). Although elimination of dihydrogen in reactions involving transition metal carbonyl clusters have been proposed earlier, we provide here, to our knowledge, the first experimental evidence for such a reaction.

Kinetic studies of the latter reaction by IR spectroscopy and stopped-flow spectrometry show that it proceeds in three stages, involving two preequilibria and a final relatively slow conversion to the products (Scheme 1). A more thorough kinetic study which aims to establish rate laws for each reaction stage as well as activation parameters is currently in progress.

5. Supplementary material

Observed and calculated mass spectra for $[Rh_2(CO)_4(\mu\text{-}SC_6H_4CH_3)_2]$ (four pages) are available on request. Crystallographic data for the structural analysis have been deposited with the Cambridge Crystallographic Data Centre, CCDC no. 143964. Copies of this information may be obtained free of charge from The Director, CCDC, 12 Union Road, Cambridge CB2 1EZ, UK (Fax: +44-1223-336033; e-mail: deposit@ccdc.cam.ac.uk or www: http://www.ccdc.cam.ac.uk).

Acknowledgements

This research has been sponsored by the Swedish Natural Science Research Council (NFR), the Swedish Engineering Research Council (TFR), The Nordic Council of Ministers, the Royal Swedish Academy of Sciences and the European Union (TMR Network Metal Clusters in Catalysis and Organic Synthesis). We thank the Wenner-Gren Center Foundation for a visiting professorship for S.P.T., Professor Lars Ivar Elding

for the generous loan of a stopped-flow spectrometer and helpful advice, Professor Anthony J. Poë for helpful discussions and Einar Nilsson for experimental assistance in the detection of dihydrogen.

References

[1] R.J. Angelici, Polyhedron (1997) 3073.
[2] H. Topsøe, B.S. Clausen, F.E. Massoth, Hydrotreating catalysis, in: J.R. Anderson, M. Boudart (Eds.), Catalysis-Science and Technology, vol. 11, Springer–Verlag, Berlin, 1996.
[3] (a) C. Bianchini, A. Meli, Acc. Chem. Res. 31 (1988) 109. (b) C. Bianchini, J.A. Casares, A. Meli, V. Sernan, F. Vizza, R.A. Sánchez-Delgado, Polyhedron (1997) 3099.
[4] M. Brorson, K. Kiriakidou, J.D. King, F. Prestopino, E. Nordlander, Metal clusters as models for hydrodesulfurization catalysts, in: P. Braunstein, L. Oro, P.R. Raithby (Eds.), Metal Clusters in Chemistry, vol. 2, Wiley–VCH, Weinheim, 1999, pp. 741–781.
[5] T.B. Rauchfuss, Prog. Inorg. Chem. 39 (1991) 259.
[6] M. Monari, R. Pfeiffer, U. Rudsander, E. Nordlander, Inorg. Chim. Acta 247 (1996) 131.
[7] K. Kiriakidou, M.R. Plutino, F. Prestopino, M. Monari, L.I. Elding, E. Valls, R. Gobetto, S. Aime, E. Nordlander, J. Chem. Soc. Chem. Commun. (1998) 2721.
[8] J.D. King, M. Monari, E. Nordlander, J. Organomet. Chem. 573 (1999) 272.
[9] S. Martinengo, P. Chini, G. Giordano, J. Organomet. Chem. 27 (1971) 389.
[10] S.P. Tunik, A.V. Vlasov, V.V. Kryvikh, Inorg. Synth. 31 (1996) 239.
[11] COLLECT, Data collection software, Enraf–Nonius, Delft, The Netherlands, 1998.
[12] Z. Otwinowski, W. Minor, Processing of X-ray diffraction data collected in oscillation mode, in: C.W. Carter, Jr., R.M. Sweet (Eds.), Macromolecular Crystallography, part A, Methods in Enzymology, vol. 276, Academic Press, 1997, pp. 307–326.
[13] G.M. Sheldrick, SHELXS-97, Program for Crystal Structure Determination, University of Göttingen, Germany, 1997.
[14] G.M. Sheldrick, SHELXL-97, Program for Crystal Structure Refinement, University of Göttingen, Germany, 1997.
[15] K. Dahlinger, A.J. Poë, P.K. Sayal, V.C. Sekhar, J. Chem. Soc. Dalton Trans. (1986) 2145.
[16] A.J. Poë, S.P. Tunik, Inorg. Chim. Acta 268 (1998) 189.
[17] E.S. Bolton, R. Havlin, G.R. Knox, J. Organomet. Chem. 18 (1969) 153.
[18] J.V. Kingstone, G.R. Scollary, J. Inorg. Nucl. Chem. 33 (1971) 4373.
[19] W. Hieber, K. Heinicke, Z. Naturforsch. Teil. B 16 (1961) 554.
[20] J. Cooke, M. Green, F.G.A. Stone, J. Chem. Soc. (A) (1968) 170.
[21] P. Kalck, R. Poilblanc, Inorg. Chem. 14 (1975) 2779.
[22] J. Pursiainen, T. Teppana, S. Rossi, T.A. Pakkanen, Acta Chem. Scand. 47 (1993) 416.
[23] C. Claver, A.M. Masdeu, N. Ruiz, C. Foces-Foces, F.H. Cano, M. Carmen Apreda, L.A. Oro, J. Garcia-Alejandre, N. Torres, J. Organomet. Chem. 398 (1996) 177.
[24] S.P. Tunik, unpublished results.
[25] G. Aullón, G. Ujaque, A. Lledós, S. Alvarez, Chem. Eur. J. 5 (1999) 1391.
[26] C.N. Wei, G.R. Wilkes, L.F. Dahl, J. Am. Chem. Soc. 89 (1967) 4792.
[27] E.R Corey, L.F. Dahl, W.J. Beck, J. Am. Chem. Soc. 85 (1963) 1202.
[28] K. Farnery, M. Kilner, J. Chem. Soc. (A) (1970) 634.
[29] N.S. Nametkin, V.D. Tyurin, M.A. Kukina, J. Organomet. Chem. 149 (1978) 355.
[30] J.A. de Beer, R.J. Haines, J. Organomet. Chem. 24 (1970) 757.
[31] B.F.G. Johnson, R.D. Johnston, P.L. Josty, J. Lewis, I.G. Williams, Nature 213 (1967) 901.
[32] B.T. Heaton, L. Strona, S. Martinengo, R.J. Goodfellow, I.H. Sadler, J. Chem. Soc., Dalton Trans. (1982) 1499.
[33] I.O. Kochevoi, S.P. Tunik, A.J. Poë, unpublished results.
[34] OMNIC spectroscopic software v. 4.1, Nicolet Instrument Corporation, Madison, Wisconsin, USA, 1997